EVALUATION OF INFRARED WELDED JOINTS OF SHORT FIBER REINFORCED THERMOPLASTICS USING DIGITAL IMAGE CORRELATION

Lucas Schraa[1*], Kai Uhlig[1], Karina Gevers[2], Volker Schöppner[2], Paul Töws[3], Julia Decker[3] and Markus Stommel[1,4]

[1] Institute of Polymer Materials, Leibniz-Institut für Polymerforschung Dresden e. V., Dresden, Germany
[2] Kunststofftechnik Paderborn, Universität Paderborn, Paderborn, Germany
[3] Fraunhofer-Institut für Betriebsfestigkeit und Systemzuverlässigkeit, Darmstadt, Germany
[4] Institut für Werkstoffwissenschaft, Technische Universität Dresden, Dresden, Germany
* Corresponding author (schraa@ipfdd.de)

Keywords: digital image correlation, infrared welding, short fiber reinforced thermoplastics, FEM

ABSTRACT

In this work, infrared welded specimens of short fiber reinforced thermoplastics are tested and the influence of different process parameters on the resulting weld strength is investigated. Two glass fiber reinforced materials with different fiber contents are used for this purpose, polyamide 6 with a glass fiber content of 50 m.% (PA6 GF50) and polyphthalamide with a glass fiber content of 35 m.% (PPA GF35). Two different preparations of tensile test specimens are investigated, unmachined specimens and specimens milled off on both sides around the weld. A high-resolution 3D-DIC system is used to further analyze the occurring effects. On the one hand, the optical strain measurement allows to visualize local material differences, on the other hand, it enables the analysis of geometry deviations, such as misalignment and angular errors, which can have a great influence on the resulting weld strength. FEM simulations are used to illustrate the influences of locally different material properties and to investigate the influence of the misalignment between the joining partners on the resulting strain field. In addition, the influence of specimen preparation on the resulting strain field is investigated by simulation.

1 INTRODUCTION

Short fiber reinforced thermoplastics are being used more and more for lightweight applications because of their high specific strength and their ability to be manufactured very economically by injection molding. However, complex geometries often require additional joining processes, such as infrared (IR) welding. Determining the mechanical properties can be challenging, as the material behavior varies locally due to different fiber arrangements and concentrations. Process-induced geometry deviations, such as misalignment and angular errors, can also change the component properties and influence the overall strain behavior. In addition, there is a reorientation of the fibers in the region of the weld and thermal load due to the infrared heating, which further causes the local properties to change. [1,2]

The 3D digital image correlation (DIC) enables a determination of the strains on the surface of the test specimen, whereby critical areas can be identified with spatial resolution even at low strains [3,4]. The measured data are also suitable for the verification of finite element method (FEM) simulations, which are often used for the design of structural components [5]. It is also possible to analyze the actual geometry of the specimens more precisely with the help of the measuring system. Schraa et al. [6] have developed a method which allows to analyze the geometry deviations of IR welded components. Thus, it was possible to determine the misalignment between the joining partners as a main influencing factor on the resulting strength of the welded joints. It was also determined that the effect of a misalignment between the joining partners is material dependent. While the strength of the welded joint for PPA GF35 decreased sharply with increasing misalignment, this effect was much less significant for PA6 GF50. One possible reason for this is a compensating influence of the weld bead, which can, however, be more or less pronounced depending on the material. Therefore, in this work, different sample preparations are made to investigate this effect in more detail.

Gevers et al. [7] further have investigated the weld characteristics of IR welded components. Thus, it was determined via micro-CT measurements that a reorientation of the fibers occurs in the weld seam caused by the welding process. Additionally, the fibers accumulate in the weld seam, which leads to a local increase of the fiber content. The mechanical effects caused by this will be investigated in more detail in this work.

2 AIM OF THE STUDY

The aim of the study is to evaluate the weld strength of infrared welded joints of short fiber reinforced thermoplastics and to demonstrate the capabilities and limitations of optical strain measurement for this purpose. The highly inhomogeneous material behavior combined with the influences of geometry deviations make the 3D-DIC an essential part of the characterization of infrared welds. Different sample preparations are investigated to allow a more accurate analysis of the weld properties. The measured strain field results from a superposition of several influencing factors, which makes it difficult to interpret the cause of the occurring effects. A special specimen preparation compensates for the geometry influence on the strain field and allows a more accurate interpretation of the material behavior in the weld area.

Furthermore, FEM simulations are carried out to interpret the effects of individual influencing factors on the measured strain field in more detail. A model developed by Schraa et al. [8] is used for this purpose. This model is able to consider the local fiber orientation as well as the local fiber concentration in order to calculate the local stiffness of the material. In this way, the effect of the welding process on the fiber distribution can be taken into account in the simulation.

3 INVESTIGATION DETAILS

In the following, the production of the test specimens and the measurement techniques used in this study are described. Two different materials were examined. Durethan BKV50H2.0 by Lanxess, a polyamide 6 with 50 m-% glass fiber content, and Ultramid Advanced N4HG7 LS BK by BASF, a polyphthalamide with 35 m-% glass fiber content. Subsequently, the experimental procedure is described. For the determination of the mechanical properties, the specimens are tested in a tensile test on a ZwickRoell 1456 tensile testing machine. To gain further information about the specimen behavior, a high-resolution 3D-DIC strain measurement system of type GOM ARAMIS is used.

3.1 Specimen preparation

First, injection-molded plates with dimensions of 130 mm x 70 mm x 3 mm were produced for the manufacture of the welded test specimens. Two plates measuring 50 mm x 70 mm x 3 mm each were taken from these plates and were then welded on their short, unmachined side. The plates were welded in dry condition. A test specimen with a constant width of 20 mm was taken from the center of each welded plate. The IR welded components are produced with various parameter sets to obtain further knowledge about the impact of different welding strategies on the resulting weld joint properties. Two different heating strategies are investigated, a gentle heating with a lower emitter intensity and a longer heating time and an intense heating with a high emitter intensity and a reduced heating time. In addition, two different joining pressures are analyzed, 1 MPa and 2 MPa. An overview of the parameter sets is shown in Table 1.

Parameter set	**A (E)**	**B (F)**	**C (G)**	**D (H)**
Material	PA6 GF50 (PPA GF35)	PA6 GF50 (PPA GF35)	PA6 GF50 (PPA GF35)	PA6 GF50 (PPA GF35)
Heating strategy	Intensive	Gentle	Intensive	Gentle
Radiator component distance [mm]	15 (12)	15 (12)	15 (12)	15 (12)
Radiator Power [%]	70	50 (45)	70	50 (45)
Heating time [s]	22 (26)	46 (82)	22 (26)	46 (82)
Joining Pressure [MPa]	1	1	2	2

Table 1: Parameter sets for the production of IR-welded components

The investigations include two different sample preparations. First, simple specimens are taken from a welded plate. This allows an estimation of the weld strength and a further analysis of the effect of geometry errors that inevitably occur in the welding process. In a second series of measurements, similar test specimens are milled off on both sides 20 mm in each direction around the weld line to a thickness of 2 mm. This preparation method on the one hand removes the weld bead and thus allows an optical strain measurement directly at the weld line. On the other hand, this technique removes the effects of a misalignment, which influences the entire strain field. An illustration of the two sample geometries is shown in Figure 1. Both preparations have advantages and disadvantages in each case, which are shown in the examinations. Before testing, the PA6 GF50 specimens were fast-conditioned according to DIN 1110, since the mechanical properties are strongly dependent on the absorbed moisture of the material [9]. The specimens made of PPA GF35 were tested in unconditioned state.

Figure 1: Specimen preparation: Top: Unmachined; Bottom: Milled-off weld region

3.2 Measurement techniques

Within the scope of these investigations, a high-resolution 3D-DIC measuring system of the type GOM ARAMIS is used for deformation measurement, to allow a detailed analysis of the local material behavior. The varying fiber orientations and concentrations lead to highly variable material properties depending on the location on the sample. These inhomogeneities can be detected and analyzed using the optical strain measurement system. In order to be able to better interpret the resulting strain distribution, this data is compared with CT measurements, which provide further information about the fiber arrangement.

In [6] a method was developed, which allows to determine geometric errors of the samples, such as misalignment or angular deviations between the joined parts. An illustration of the geometry deviations is shown in Figure 2.

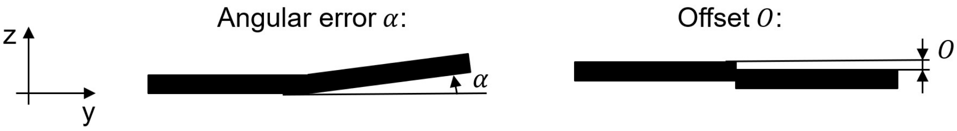

Figure 2: Possible geometry deviations of the welded specimens

To quantify the offset and angular error between the joining partners the 3D-DIC data is used to get the necessary information of the surface coordinates. Therefore, a reference picture was taken for every specimen clamped only on one side to consider a stress-free state. The position data were exported and further processed in Python. To analyze the geometry a function was set up which consists of two linear functions separated by a vertical line at the weld line position y_{SN}:

$$z(y) = \begin{cases} m_1 \cdot y + n_1 , & y < y_{SN} \\ m_2 \cdot y + n_2 , & y > y_{SN} \end{cases} \tag{1}$$

A residual was calculated between the y-z coordinates from the optical strain measurement ($y_i^{Measure}, z_i^{Measure}$) and the set-up function $z(y)$. By minimizing the residual, this function can be fitted to the measurement data in such a way that the two linear functions represent the surface of the joining partners and the vertical line approximates the position of the weld seam y_{SN}.

$$res = \sum_{i=1}^{n} \left(z_i^{Measure} - z\left(y_i^{Measure}\right)\right)^2 \tag{2}$$

The minimization of the residual was done using a differential evolution algorithm. The advantage is beside the simplicity of the algorithm that the global minimum is reliably found regardless of the chosen initial values [10].

The offset O between the joining partners was calculated after optimization using the difference of the function values at the weld position. The angular error α is calculated via the slope of the approximated functions:

$$O = |(m_2 \cdot y_{SN} + n_2) - (m_1 \cdot y_{SN} + n_1)| \tag{3}$$

$$\alpha = arctan(|m_2 - m_1|) \tag{4}$$

Figure 3 shows an example of the result of the geometry analysis for a test specimen. The measuring points of the digital image correlation are shown in blue. The orange line shows the solution of the optimized approximation function. The weld position of the model is shown in black. For this example an offset of 0.28 mm and an angular error of 1.2° was calculated.

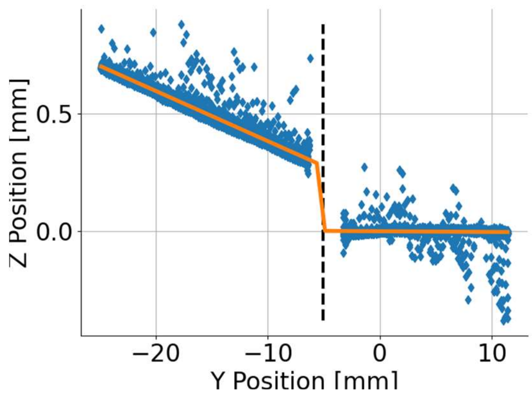

Figure 3: Result of the geometry detection for a welded specimen

4 RESULTS

In the following, the results of this work are presented. First, the resulting mechanical properties of the welded specimens are shown. Then, in order to analyze the findings in more detail, the results of the optical strain measurements are presented. Last but not least, the measured strain fields are compared with the results of FEM simulations.

4.1 Mechanical Properties

In this chapter, the mechanical properties determined based on the testing machine data are investigated. The results are shown in Figure 4. The cross section that is necessary for the calculation of the tensile strength is measured next to the weld seam. Therefore, the higher cross section induced by the weld bead is not considered in the calculated values. The top diagrams show the tensile strength of PA6 GF50 for both specimen preparations, on the left the unmachined geometry and on the right the milled-off specimens. The different welding strategies are distinguished by color. For the unmachined specimens a slightly higher tensile strength is visible for a joining pressure of 1 MPa compared to 2 MPa.

Additionally, a gentle heating strategy results in a small increase in the weld strength compared to an intensive heating strategy for both joining pressures. The results of the milled-off specimens show a similar tensile strength for all welding strategies. This indicates that the process parameters mostly influence the factors on the tensile strength, which are only present in the unprocessed specimens. The weld bead, for example, leads to a larger specimen cross section in the critical area of the specimen, at the weld line. Thus, a possible cause could be a variation in the strength of the bead material depending on the process parameters. The higher the residual strength of the bead material, the greater the supporting effect on the overall strength of the respective specimen. Another influencing factor on the resulting tensile strength that is only affecting the results of the unmachined specimens is the offset between the joining partners.

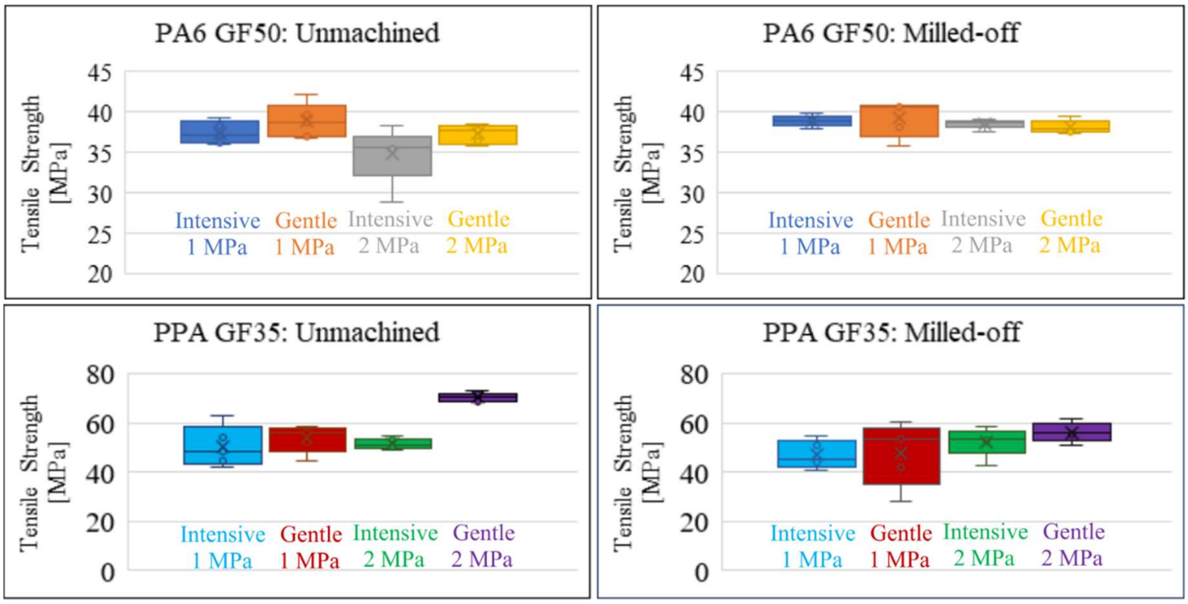

Figure 4: Tensile strength of the IR-welded specimens: Top: PA6 GF50; Bottom: PPA GF35; Left: Unmachined; Right: Milled-off

The results for PPA GF35 are shown in the bottom diagrams in Figure 4. In the left diagram for the unprocessed specimens a higher mean tensile strength for a gentle heating strategy is visible compared to the intense heating for both joining pressures, similar to PA6 GF50. However, the specimens fabricated with a gentle heating strategy and a joining pressure of 2 MPa show a much higher strength compared to the other parameter sets. Since this effect is not as pronounced for the milled specimens, this again indicates that the strength is likely dependent on the offset between the joining partners or residual strength of the bead material.

To consider additional factors when interpreting the results, the geometric deviations (angular error and offset between the joining partners) were calculated using the DIC data with the method described in chapter 3.2. The results are shown in Table 2. For each parameter set, the mean value and the standard deviation are given.

Parameter set		A	B	C	D	E	F	G	H
Offset [mm]	mean	0.33	0.26	0.49	0.35	0.20	0.15	0.27	0.06
	std	0.04	0.10	0.35	0.01	0.07	0.05	0.07	0.03
Angular error [°]	mean	0.25	0.26	0.32	0.18	0.98	0.42	1.22	0.26
	std	0.28	0.12	0.49	0.13	0.05	0.31	0.74	0.22

Table 2: Measured geometric deviations for each parameter set

For PA6 GF50 (A-D) an average offset of 0.36 mm was measured. The highest offset was measured for parameter set C, which shows the lowest tensile strength in Figure 4. Parameter set B, which shows the highest tensile strength, has the lowest measured offset. This indicates a distinct negative influence of the offset between the joining partners on the resulting tensile strength of the specimen.

The average offset of the specimens made of PPA GF35 (E-H) is 0.17 mm, while the specimens produced with gentle heating and 2 MPa joining pressure, which show an exceptionally high tensile strength, have a much lower average offset of 0.06 mm. This again shows the negative influence of the misalignment on the resulting weld strength. Especially for PPA GF35, the angular error seems to correlate with the offset of the parameter sets. Therefore, there may be a causal relationship between the two effects. In the following, a more detailed analysis of the strain fields measured by DIC is given.

4.2 Analysis by Digital Image Correlation

The two different sample preparations provide various advantages and disadvantages when using DIC, which will be elaborated in the following. Figure 5 shows a comparison of both specimen preparations for PA6 GF50. The left figure shows the strain distribution in the tensile direction for an unprocessed specimen with an applied strain of 2 %. It is visible that the strain field is very inhomogeneous. The upper joining partner appears to deform significantly more than the lower joining partner. In the center of the specimen, the weld bead can be seen, which is not detected by the optical strain measurement system. Thus, the weakest region around the weld line cannot be analyzed. Nevertheless, the unmachined specimens provide the essential strength values for the component design, since the weld beads are usually not subsequently removed in real component applications.

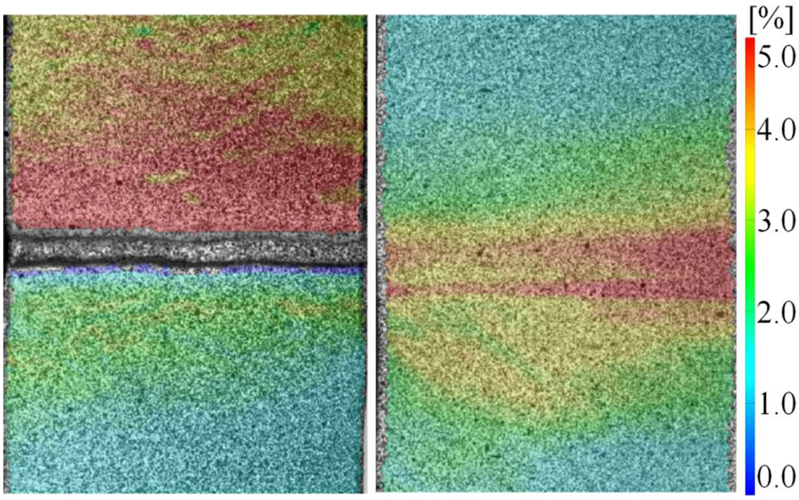

Figure 5: Comparison of the strain field in tensile direction of two different specimen preparations for PA6 GF50: Left: Unmachined; Right: Milled-off

In Figure 5 on the right the strain field of a specimen with a milled-off weld region is shown. In this case the applied strain is at 1.5 %. As can be seen, the strain field is now much more symmetrically distributed around the weld, suggesting that the strain differences in the joining partners of the unmachined specimen are caused by geometry errors, such as the misalignment between the joining partners. The influence of these geometry errors is removed by the subsequent machining of the specimens, which allows a much better interpretation of the local material behavior. A strong strain concentration around the weld is now visible. This effect was for the unmachined specimen superimposed by the influence of geometry deviations and the weld area was covered by the weld bead, which prevented an analysis of this area. Several causes can be considered for this strain concentration. The weld zone of the joining partners originally comes from the boundary region of the injection-molded plate. Since a shear flow is predominant in the boundary region during the flow process, the fibers are oriented in the flow direction and thus orthogonal to the subsequent loading direction. In the central area of the injection molded sheet, on the other hand, a middle layer is present in which the fibers orient themselves orthogonally to the flow direction and thus in the direction of the subsequent loading direction, resulting in significantly higher stiffness in loading direction.

In Figure 6 the strain fields in tensile direction of the two different specimen preparations are shown for PPA GF35. The applied strain for both specimens is 1 %. In comparison to the results of PA6 GF50 the strain fields are much more homogeneous for both specimen types. One reason for that is the lower fiber content of PPA GF35. The differences in the local stiffness are likely caused by the local variation of the fiber orientation, as described previously. However, the impact of this effect decreases with lower fiber content. For the unmachined specimen a strain concentration at the upper side of the weld is visible, which might again be caused by the offset between the joining partners. For the milled-off specimen, the average strain in the measured area is slightly higher. This is caused by the smaller cross section in the milled off area compared to the outer regions, which results in a strain concentration in the measuring area.

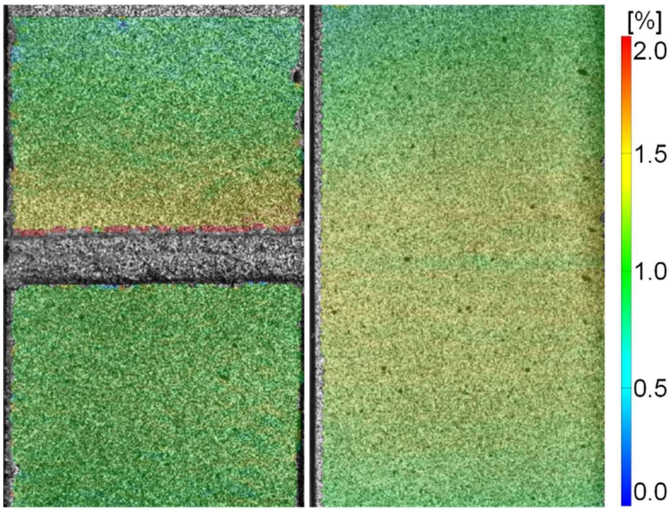

Figure 6: Comparison of the strain field in tensile direction of two different specimen preparations for PPA GF35: Left: Unmachined; Right: Milled-off

Figure 7 shows CT images of one representative specimen each for PA6 GF50 (left) and PPA GF35 (right). The intensity measured on the detector is shown qualitatively. The intensity can be used to visualize density differences in the material, which provide information about the local concentration of the fibers. Thus, due to the higher density of the fibers, a higher concentration of fibers can be assumed in areas of lower intensity. For PA6 GF50, a comparison with the measured strains in Figure 5 indicates that the strain concentration in the weld region could also be partly related to a lower concentration of fibers in this area. The CT image of the PPA GF35 specimen shows a much more uniform fiber distribution, which is also confirmed by the significantly more homogeneous strain field in Figure 6.

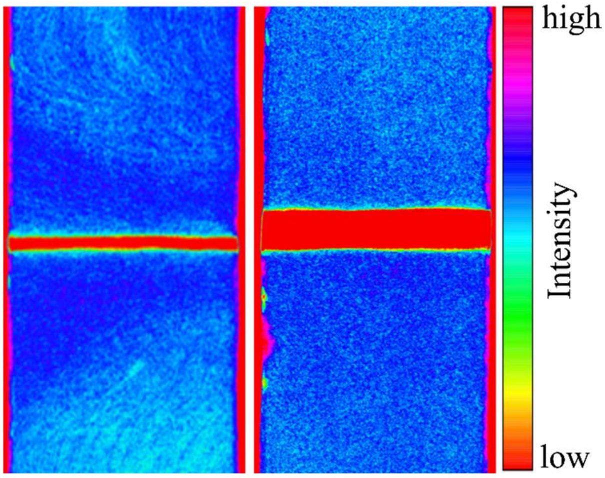

Figure 7: CT-Images of one representative specimen for each material: Left: PA6 GF50; Right: PPA GF35

4.3 Simulation of the Identified Influencing Factors

In this chapter, FEM simulations are performed to gain further insight into the main factors influencing the specimen behavior and the measured strain field. In the simulation, these influencing factors can be observed individually, so that they can also be evaluated independently, while in the measurement, all influences together produce one single result. Using the milled-off samples, it could be shown that the material behavior is strongly inhomogeneous. A major influencing factor is the local orientation of the fibers in the material. By examining the unprocessed specimens, it was also possible to determine that the offset between the joining partners also has a strong influence on the strain field. These two factors will be investigated by simulation in the following using PA6 GF50 as an example.

For the consideration of the local material stiffnesses, a homogenized material model is used, which was developed in [8]. In the model, the stiffness matrix for an anisotropic elastic material model is calculated via the material parameters of the fiber and matrix material, as well as the information of the local fiber orientation, the fiber content and the geometry of the fibers. The necessary information about the local fiber orientation is obtained from an injection molding simulation of the original injection molded plate. Since the fiber orientation in the weld seam changes in the downstream joining process and thus the injection molding data can no longer be used at this point, fiber orientations measured in CT investigations from [7] in the area of the weld seam are transferred to the model. In order to consider the locally varying concentration of the fibers, the results of a series of measurements by thermogravimetric analysis from [8] are applied to the simulation model. To analyze the effect of the misalignment on the strain field in more detail, the weld bead is neglected in the simulation. Linear hexahedral elements with an edge length of 0.5 mm were used for meshing the parts.

Figure 8 compares the results of different simulations. All models were loaded with 1 % applied strain. On the left, an ideally welded specimen is shown, which has no misalignment between the joining partners. Only the locally different material properties lead to a slight strain concentration in the area of the weld. In the middle picture, an additional offset of 0.34 mm is applied. The offset in the weld area also causes a misalignment of the clamping positions, which was considered in the simulations. It is visible that, similar to the results of the optical strain measurement in Figure 5, there is now a strain concentration above the weld seam, while there is a significantly lower strain apparent below the weld seam. The strain field is now superimposed with a geometry effect, which complicates the interpretation of the local material properties. In the right picture, the geometry of the specimen with the applied offset in the measuring area was reduced to 2 mm thickness, as it was done with the milled-off test specimens. It can be seen that now the strain field is much more symmetrical. The simulation supports the assumption that this specimen preparation removes the effect of the misalignment on the strain field. In comparison with the left image, however, it is noticeable that the processing nevertheless changes the properties of the specimen. Because the measuring area now has a smaller cross-section, the total strain in this area increases. In addition, the strain concentration around the weld seam is significantly more pronounced compared to the unmachined defect-free specimen in the left image. One reason for this is that the subsequent machining removes the outer layers of the specimen, which have a significantly lower stiffness due to the fiber orientation being orthogonal to the tensile direction, than the remaining middle layer, which has a main fiber orientation in the tensile direction. This should be taken into account when interpreting the results of the DIC measurements.

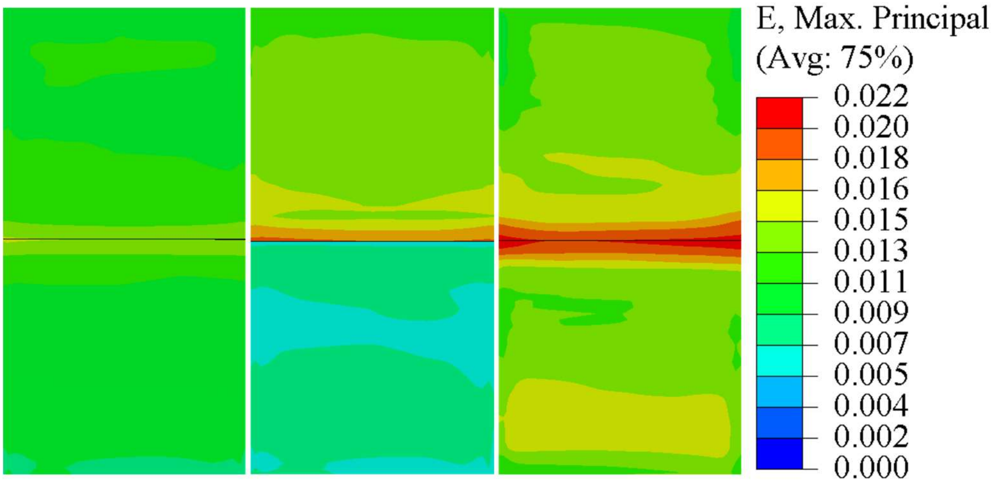

Figure 8: Results of different simulation models at 1 % applied strain: Left: Unmachined geometry, Middle: Unmachined geometry with misalignment, Right: Milled-off misaligned geometry

5 CONCLUSION AND OUTLOOK

In this work, infrared welded joints of the materials PA6 GF50 and PPA GF35 were investigated with different process settings. Two different specimen preparations were used for this purpose. The results showed a higher weld strength for PA6 GF50 for gentle heating compared to intensive heating and for a lower joining pressure of 1 MPa compared to 2 MPa. Comparing the two preparation strategies, it was found that one cause for the difference in strength is likely the supporting effect of the weld bead. Using a high-resolution 3D DIC system, it was possible to quantify geometry deviations such as angular errors and misalignment between the joining partners. A negative effect of the misalignment between the joining partners on the weld strength was found by comparing the measured deviations with the resulting weld strengths. The evaluated strain fields showed that the geometry misalignments significantly affect the strain distribution on the measured surface. Milling off the specimens in the measurement area prevents this effect. FEM simulations were used to show the influence of local material inhomogeneities without an effect of geometric deviations on the strain field. In addition, it was shown how the different specimen preparations can affect the measured strain field. The results of the simulations provided good agreements with the measured strain fields.

Future studies should further investigate the properties of the weld bead. This work provides evidence that the different welding process parameters affect the mechanical properties of the bead material. The weld bead appears to have a supporting effect and influence the resulting weld strength. It would also be interesting to further investigate the cause of the geometry deviations and whether there is a correlation of the resulting misalignment and angular errors with the process parameters.

ACKNOWLEDGEMENTS

The IGF project no.: 21276N of the Research Association of Automotive Technology (FAT) belongs to the German Association of the Automotive Industry (VDA), Behrenstraße 35, 10117 Berlin. The research project was funded by the AiF within the program for sponsorship by Industrial Joint Research (IGF) of the German Federal Ministry of Economic Affairs and Climate Action based on a decision by the German Bundestag.

Supported by:

Federal Ministry for Economic Affairs and Climate Action

on the basis of a decision by the German Bundestag

REFERENCES

[1] I. Fiebig and V. Schöppner, Influence of the initial fiber orientation on the weld strength in welding of glass fiber reinforced thermoplastics. *International Journal of Polymer Science*, 2016, pp. 1-16.

[2] R. Fuhrich, *Strahlungserwärmung beim Kunststoffschweißen mit Infrarotstrahlung*, Schlussbericht zum AiF-Forschungsprojekt 15971 BR, 2011.

[3] M. Schuth and W. Buerakov, *Optische Messtechnik – Praktische Anwendungen für Entwicklung*, Carl Hanser Verlag, 2017.

[4] V. Crupi, et al., Experimental analyses of SFRP material under static and fatigue loading by means of thermographic and DIC techniques, *Composites Part B*, **77**, 2015, pp. 268-277.

[5] N. Z. Miloševic, et al., Determination of the actual stress–strain diagram for undermatching welded joint using DIC and FEM, *materials*, **14**, 2021, 4691, pp. 1-14.

[6] L. Schraa, et al., Bewertung von IR-Schweißverbindungen an kurzfaserverstärkten Thermoplasten mittels digitaler Bildkorrelation, *Werkstoffe und Bauteile auf dem Prüfstand, 40. Vortrags- und Diskussionstagung Werkstoffprüfung 2022 (Ed. M. Zimmermann), Dresden, Oktober 2022.* Tagungsband zur Werkstoffprüfung 2022, vol. 40, pp. 169-175, DGM - Deutsche Gesellschaft für Materialkunde e.V., 2023.

[7] K. Gevers, et al., Effects of different heating strategies on the quasi-static and cyclic load-bearing capacities of infrared-welded, glass-fibre-reinforced thermoplastic components, *Joining Plastics,* **16**, 2022, pp. 182-189.

[8] L. Schraa, et al., Simulation of infrared welded short fiber reinforced thermoplastic parts based on Mori-Tanaka homogenization method, *Advanced Structured Materials*, Springer (accepted)

[9] DIN EN ISO 1110: Polyamide – Beschleunigte Konditionierung von Probekörpern, 2019.

[10] R. Storn and K. Price, Differential Evolution – A Simple and Efficient Heuristic for Global Optimization over Continuous Spaces, *Journal of Global Optimization*, **11**, 1997, pp. 341-359.